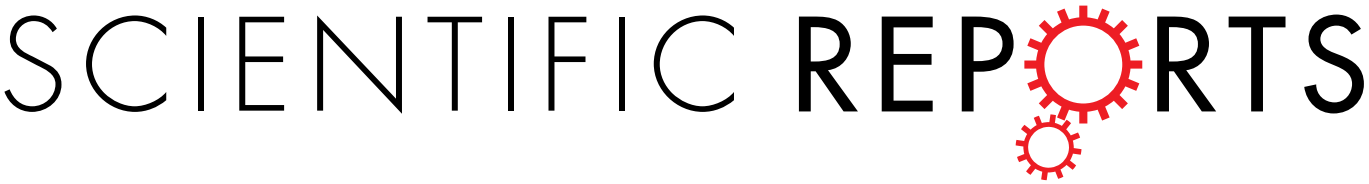

OPEN

Optical characterization of red blood cells from individuals with sickle cell trait and disease in Tanzania using quantitative phase imaging

Received: 11 May 2016
Accepted: 22 July 2016
Published: 22 August 2016

JaeHwang Jung[1,*], Lucas E. Matemba[2,*], KyeoReh Lee[1], Paul E. Kazyoba[3], Jonghee Yoon[1], Julius J. Massaga[3], Kyoohyun Kim[1], Dong-Jin Kim[4] & YongKeun Park[1,5]

Sickle cell disease (SCD) is common across Sub-Saharan Africa. However, the investigation of SCD in this area has been significantly limited mainly due to the lack of research facilities and skilled personnel. Here, we present optical measurements of individual red blood cells from healthy individuals and individuals with SCD and sickle cell trait in Tanzania using the quantitative phase imaging technique. By employing a quantitative phase imaging unit, an existing microscope in a clinic is transformed into a powerful quantitative phase microscope providing measurements on the morphological, biochemical, and biomechanical properties of individual cells. The present approach will open up new opportunities for cost-effective investigation and diagnosis of several diseases in low resource environments.

Sickle cell disease (SCD) is an autosomal genetic blood disorder from the inheritance of point-mutated globin genes producing abnormal hemoglobin (Hb)[1]. Under deoxygenated conditions, the abnormal hemoglobin, also known as hemoglobin S (HbS), become self-assembled inside red blood cells (RBCs), which results in the formation of rigid fibril structures. These fibril structures cause damages to the cell membrane making RBCs less deformable and can even change RBCs into sickle shapes. Stiffened RBCs in patients with SCD damage endothelial cells and even cause the occlusion of microvascular structures[2]. Thus, patients with SCD suffers severe anemia, pain, devastating disabilities, and in some cases, premature death[3,4]. In contrast, individuals with sickle cell trait (SCT), the heterozygous condition of SCD, do not exhibit apparent health issues. Without genetic analysis, the SCT individuals are hardly distinguished from healthy individuals. Rarely, severe clinical manifestations including exertional rhabdomyolysis (the rapid breakdown of skeletal muscle due to injury to muscle tissue) have been reported in individuals with SCT under extreme conditions such as severe dehydration and high-intensity physical activity[5,6].

According to the World Health Organization, approximately 4.5% of the world population carries the sickle genes[7]. The sickle genes are found more frequently in the tropics, especially in Sub-Saharan Africa. For example, the prevalence of the sickle genes in Tanzania is estimated to be 13% and even up to 50% among some ethnic groups[8,9]. The mortality of infants with SCD is as high as 90% in areas with limited medical facilities and 50% in areas with improved health infrastructures[10] while only 1% of the infants with SCD dies in the United States[11]. The high prevalence of sickle genes imposes heavy economic and clinical burdens on Sub-Saharan Africa countries. Although genetic and biochemical information about SCD and SCT have been well understood, mechanical properties of these diseases have not been fully investigated. Measuring and understanding the mechanical properties of SCD and SCT RBCs are crucial to comprehend the mechanisms of diseases and evaluate the efficacy

[1]Department of Physics, Korea Advanced Institute of Science and Technology, Daejeon 34141, Republic of Korea. [2]National Institute for Medical Research, P.O. Box 476, Morogoro, Tanzania. [3]National Institute for Medical Research, 3 Barack Obama Drive, P.O. Box 9653, 11101 Dar es Salaam, Tanzania. [4]Nelson Mandela African Institution of Science and Technology, School of Life Science and Bioengineering, P.O. Box 447 Arusha, Tanzania. [5]TomoCube, Inc., Daejeon 34051, Republic of Korea. *These authors contributed equally to this work. Correspondence and requests for materials should be addressed to D.-J.K. (email: djkim.nmaist@gmail.com) or Y.P. (email: yk.park@kaist.ac.kr)

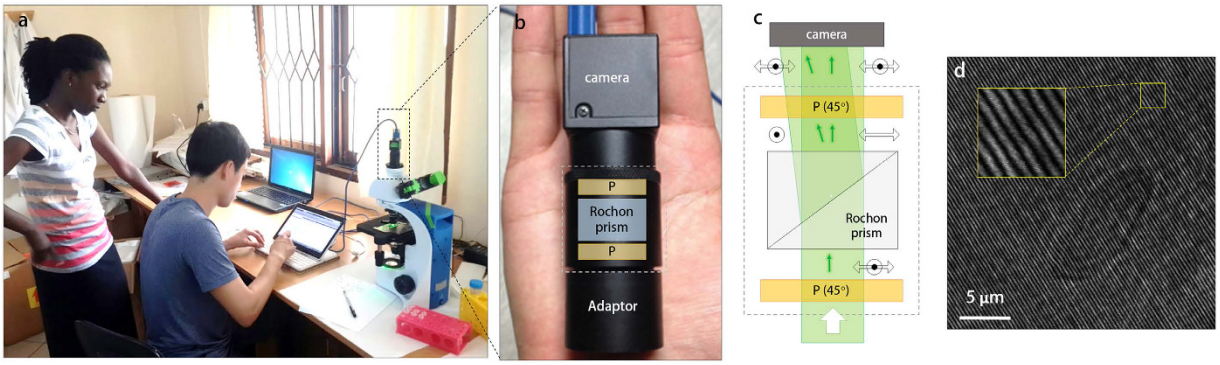

Figure 1. Principle and demonstration of the quantitative phase imaging unit (QPIU). (**a**) A photograph of experiments performed at a local clinic in Tanzania using the QPIU. (**b**) A photograph and (**c**) schematic of the QPIU. The QPIU consists of a Rochon prism and two parallel linear polarizers (P). The green and the black arrows indicate the optical paths and polarization direction, respectively. (**d**) A recorded hologram of a sickle-shaped RBC. The inset shows the magnified interference pattern.

of drugs and medical treatments targeted to relieve the complications of the diseases. However, these kinds of studies have been mostly performed in developed countries in US or Europe, mainly due to accessibility and well equipped medical research facilities. Unfortunately, research in these developed countries may not reflect situations in Sub-Saharan Africa because it is difficult to find and access untreated samples in the developed countries. The patients in the developed countries take medical treatments which could influence the properties of the RBCs. For example, hydroxyurea increases the presence of fetal heloglobin (HbF) in place of HbS and HbF does not cause sickling and presumably the mechanical properties of RBCs[12]. In addition, chronic blood transfusion, another common treatment for severe cases, adds foreign RBCs without HbS and also changes the average characteristics of the RBC population. Considering theses asepcts, the investigation of SCD and SCT in Sub-Saharan Africa can provide valuable information to understand the diseases. Despite the devastating burden of SCD, unfortunately, there have been insufficient investigations regarding SCT and SCD across the region due to the lack of funds, facilities, and experts. Hence, it is high time to develop and transfer simple, cost-effective and easy-to-use technology to help study the disease and build their knowledge about SCT and SCD. For a better understanding of SCD, SCT, and their complications, various technical approaches have been demonstrated mostly focusing on the mechanical properties of RBCs[12]. The mechanical properties of SCD RBCs have been measured based on invasive or force-applying techniques including micropipette aspiration[13] and filtration[14] as well as a flow-controlled chamber[15], optical tweezers[16], and atomic force microscope[17]. Although all these techniques have undoubtedly improved the understanding of the relation between SCD and the mechanical properties of the RBCs, simultaneous investigations of the multiple properties of individual cells are still required to better understand the diverse interactions of the mechanical, biochemical, and morphological characteristics.

Recently, quantitative phase imaging (QPI) techniques have been introduced to study the morphology and mechanical properties of individual SCD RBCs[18,19]. QPI is an interferometric microscopy technique capable of measuring optical phase delays of biological cells and tissues noninvasively and quantitatively[20,21]. However, most QPI techniques require complicated, sensitive, and bulky optical instrumentation which has to be operated and occasionally aligned by well-trained personnel. Therefore, all the previous studies with QPI have been performed at research facilities collaborating with medical hospitals in developed countries. This constraint is unfortunate because QPI has much to offer the fields of SCD and SCT with its unique single-cell profiling capability and label-free and quantitative imaging ability, particularly for the study of RBC-related pathophysiology[22–28].

Here, we report the investigation of SCD and SCT RBCs in Africa using QPI. Exploiting a recently developed quantitative phase imaging unit (QPIU)[29], an existing simple bright-field microscope in a local clinic in Tanzania was converted into a highly precise and sensitive QPI instrument. We note that the objectives of this study are (1) to demonstrate the capability of QPI techniques in African countries regarding technical development and (2) to perform systematic measurements and comparative analyzes of individual RBCs from healthy, SCD, and SCT patients as scientific advances. Using the QPIU, we performed optical measurements on the morphological, biochemical, and mechanical properties of individual RBCs collected from individuals with SCD and SCT. The quantitative characteristics of the RBCs including the aspect ratio, membrane curvature, Hb contents, and membrane fluctuation were measured from the quantitative phase images. In total, 623 RBCs from 23 individuals (5 healthy, 8 SCT, and 10 SCD donors) were measured, and their morphological, biochemical, and mechanical properties were systematically analyzed. We found that both the RBCs from SCD and SCT patients had significantly different morphological and biomechanical properties compared to the healthy RBCs. The demonstration of the QPIU in Tanzania will provide new opportunities for the cost-effective and quantitative investigation of SCD as well as other neglected tropical diseases in low- and middle-income countries.

Results

Experimental setup. To perform QPI in Tanzania, a standard bright-field optical microscope was converted into a highly stable and precise quantitative phase microscope with a QPIU (Fig. 1a). The QPIU is compact, simple, robust and easy-to-use. The QPIU consists of only three optical components: two linear polarizers and

a Rochon prism (Fig. 1b). The unit can be attached to the image port of a standard microscope, and it does not require optical alignment. The principle behind the QPIU is lateral-shearing common-path interferometry[29]. Briefly, a beam from the image port of the microscope is first linearly polarized and then split into two beams with different propagation directions with a polarization prism (Fig. 1c). The polarization states of the two beams are matched to be parallel with the polarizer placed after the prism. Then, a spatially modulated interferogram is generated at an overlapped region of the two beams at the CCD plane (Fig. 1d). From the measured interferogram, an optical field image consisting of both the amplitude and phase map is retrieved using a field-retrieval algorithm[30].

In this experiment, a Rochon prism was used for the polarizing prism, instead of a Wollaston prism, which was used in a previous paper[29]. Whereas a Wollaston prism deviates both polarized beams from an optical axis, a Rochon prism deviates only one polarized beam. Thus, the use of the Rochon prism further simplifies the optical system of the QPIU because a CCD plane can be adjusted as perpendicular to the optical axis and not perpendicular to the direction of one of the deviated beams. The two polarizers are rotated so that the polarization direction of the polarizers have a 45° angle to the polarization axes of the beams, which ensures the maximum image contrast of the interferogram patterns and thus the maximum signal-to-noise ratio of the measurements. The Rochon prism and two polarizers are precisely adjusted and compactly assembled in an aluminum tube, which is mounted in front of a CCD camera (FL3-U3-32S2M-CS, Point Grey). As an illumination source, a laser diode (CPS532, $\lambda = 532$ nm, Thorlabs Inc.) is installed on a bright-field microscope (B-382PLi-ALC, Optika) equipped with a 100× oil immersion objective (NA = 1.25, M-148, Optika). We note that the QPIU is compatible with both upright and inverted microscopes, and the choice of an objective lens is arbitrary. The detailed designing parameter for QPIU can be found elsewhere[29].

The QPIU system is highly stable even when all the experiments were performed on a typical office desk. The temporal stability of the QPIU system, defined as the standard deviation value of background over time, was 9.4 nm, which is comparable to the 7 nm of fluctuation noise in a recent common-path interferometric system on a scientific-grade anti-vibration optical table[31]. This highly stable QPIU system is also cost-effective. The total cost of building a QPIU microscope is less than $3,000 USD including the microscope, the laser source, the camera and QPIU while a typical quantitative phase microscope system costs more than $30,000 USD. The cost only for the QPIU is less than $1,000 USD. This cost could be further decreased when the QPIU is commercially optimized, for example, via mass production and using cheaper materials for a main body.

Classification of the RBCs. RBCs were collected at a medical center in Tanzania from 23 individuals (5 healthy, 8 SCD, and 10 SCT). At least 17 RBCs per participant and 623 RBCs were measured. The classifications of individuals into healthy, SCD, and SCT were confirmed with Genotyping by sequencing with polymerase chain reaction (See *Methods*). We categorized the collected RBCs into four groups: healthy RBCs, SCT RBCs, irreversibly sickled SCD cells (ISCs), and reversibly sickled SCD cells (RSCs). There are 149, 286, 34, 154 RBCs in healthy, SCT, ISC, and RSC groups, respectively. In this study, we considered each cell as a single data and excluded top and bottom 3% population to remove outliers. The measured data for individual donors are tabulated and statistical analysis using the mean values of individual donors are presented in Supplementary Table S1 and Figures S1–4, respectively.

The RBCs from individuals with SCD were separated into the RSC and ISC groups depending on their shapes because they had distinguishable shapes and were expected to have different characteristics. Under oxygenated conditions, some RBCs in SCD patients remain sickle shapes due to permanently damaged membranes. These permanently deformed RBCs are considered as ISCs and usually have dense Hb concentration and reduced deformability[32]. Other RBCs that recover discoid shapes are called RSCs. As the RSCs suffer repeated transforms and accumulate damage on membranes, the cells become ISCs losing some ions and water but not Hb. The distinction of the ISCs and RSCs was achieved by visual inspections done by a trained medical doctor. The other RBCs from individuals with SCD were in discocyte shapes and considered as RSCs because the SCD patients in this study had not received a blood transfusion. SCD patients who receive a blood transfusion would have a population of healthy cells in the sample as well. Although the RBCs from SCD patients can be further classified into four subtypes based on their Hb concentration[33,34], we used the two classifications for SCD RBCs mentioned above mainly due to the lack of equipment for the separation in the clinic.

Topography of the RBCs. To demonstrate the capability of precise individual cell imaging, we performed quantitative phase imaging of the collected RBCs at the medical center in Tanzania. For each cell, 240 interferograms were recorded at a frame rate of 60 Hz with the QPIU. The optical phase image $\Delta\phi(x, y, t)$ is retrieved from a measured interferogram using a field retrieval algorithm[30]. Then, the height map of a cell $h(x, y, t)$ is calculated from $\Delta\phi(x, y, t)$ using the relation $\Delta\phi(x, y, t) = 2\pi/\lambda \cdot \Delta n \cdot h(x, y, t)$, where λ is the wavelength of light in a vacuum, and Δn is the refractive index contrast between a RBC and the medium (See *Methods*).

The representative cell height maps are shown in Fig. 2a–d for the healthy, SCT, ISC, and RSC groups, respectively. Healthy RBCs exhibited characteristic discocyte shapes (Fig. 2a). SCT RBCs also showed discocyte shapes similar to the healthy RBCs (Fig. 2b). ISCs exhibited distinct sickle shapes whereas the RSCs had discocyte shapes (Fig. 2c–d).

Dynamic membrane fluctuations of the RBCs. To investigate the biomechanical properties of individual RBCs in SCD and SCT, we addressed the dynamic membrane fluctuations in the cell membranes. Dynamic membrane fluctuations in RBCs, with the displacement of tens of nanometers at millisecond temporal dynamics, are strongly related to the deformability of RBCs. These dynamic membrane fluctuations in RBCs have been quantitatively and precisely measured using QPI techniques[35–38], especially for the study of the effects of diverse pathophysiological conditions and the deformability of RBCs, including osmotic pressure[39], morphology[23],

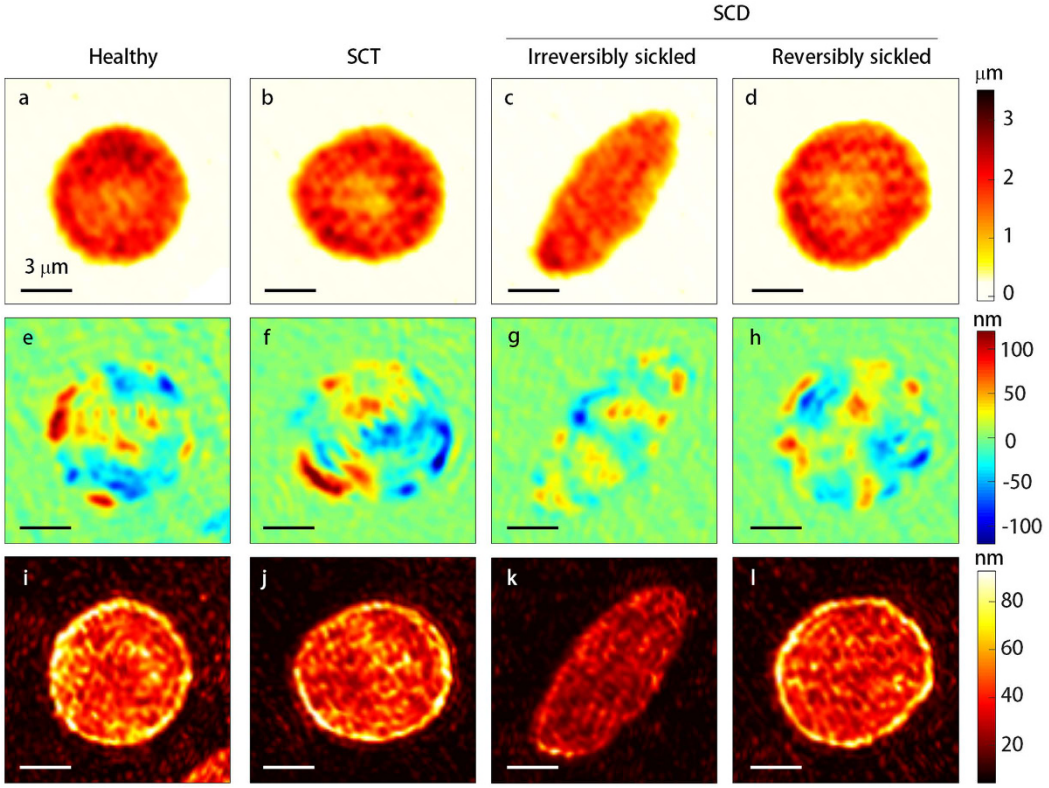

Figure 2. Shapes and fluctuations of RBCs. Height (the top row; **a–d**), instantaneous membrane displacement (the middle row; **e–h**), and magnitidue of fluctuation (the bottom row; **i–l**) map of a RBC from a healthy individual (**a,e,i**), a RBC from an individual with SCT (**b,f,j**), an irreversibly sickled RBC (**c,g,k**) and a reversibly sickled RBC (**d,h,l**) from an individual with SCD, respectively.

ATP[22], malaria[24,40,41], babesiosis[26], and cord blood[42]. Among them, QPI techniques have been previously used to measure dynamic membrane fluctuations in RBCs from patients with SCD[18,19].

To address the dynamic membrane fluctuations in RBCs, dynamic displacements of the cell height maps $\Delta h(x, y, t)$ are obtained by subtracting the instantaneous height maps from the temporal averaged height map as $\Delta h(x, y, t) = h(x, y, t) - \langle h(x, y, t)\rangle_t$. The representative instantaneous height displacement maps are shown in Fig. 2e–h for the healthy, SCT, ISC, and RSC groups, respectively. Healthy RBCs had high membrane fluctuations, implying large deformability (Fig. 2e), and SCT and RSC RBCs also showed comparable but slightly decreased deformability (Fig. 2f,h). However, ISCs exhibited significantly decreased dynamic membrane fluctuations, compared to the other groups, suggesting reduced deformability (Fig. 2g). Corresponding magnitudes of the membrane fluctuation, which were calculated as standard deviation of the dynamic membrane displacement, were presented in Fig. 2i–l.

Analysis of the morphological and biomechanical properties of the RBCs. To systematically investigate the alterations associated with SCT and SCD, the morphological and biomechanical parameters of the RBCs were retrieved from individual RBCs, including the aspect ratio, cell membrane curvature, and membrane fluctuations (Fig. 3). The aspect ratio was calculated by the ratio of diameters along the long and short axes of a cell. The long and short axes of a cell were found by fitting an ellipse to the cell boundary (See Supplementary Information). The healthy and SCT RBCs had symmetric shapes. The ISCs presented significantly decreased aspect ratios due to the sickled shapes. The RSCs showed slight decreases in the aspect ratios compared to the healthy and SCT RBCs. The mean values of the aspect ratios were 0.89 ± 0.08, 0.90 ± 0.06, 0.44 ± 0.07 and 0.81 ± 0.12 (mean $\pm$ standard deviation) for the healthy, SCT, ISC, and RSC groups, respectively (Fig. 3a). The analysis that was obtained using mean values of individual donors instead of each cell data also presented comparable results (Supplementary Figure S1).

To study whether a dimple shape is maintained, the curvature of the cell membrane was calculated from the measured cell height map (See *Methods*). The dimple shape in healthy RBCs was maintained by the intact spectrin cytoskeletal structures and membrane-bound proteins. It is known that polymerized HbS can cause damages to the cortex structures of the RBC membrane[43]. The damaged membrane could result in the change of a dimple curvature. The mean values of the curvature are -0.133 ± 0.13, -0.169 ± 0.10, -0.054 ± 0.17 and $-0.202 \pm 0.12\,\mu m^{-1}$ for the healthy, SCT, ISC, and RSC groups, respectively (Fig. 3b). The results show that the SCT RBCs and RSCs have dimple shapes in the middle of the cell membrane, whereas the ISCs lost their dimple shapes. The statistical analysis using mean values of individuals instead of every cell data also presents ISCs have significantly flattened curvatures compared to RSCs. as shown in the Supplementary Figure S2.

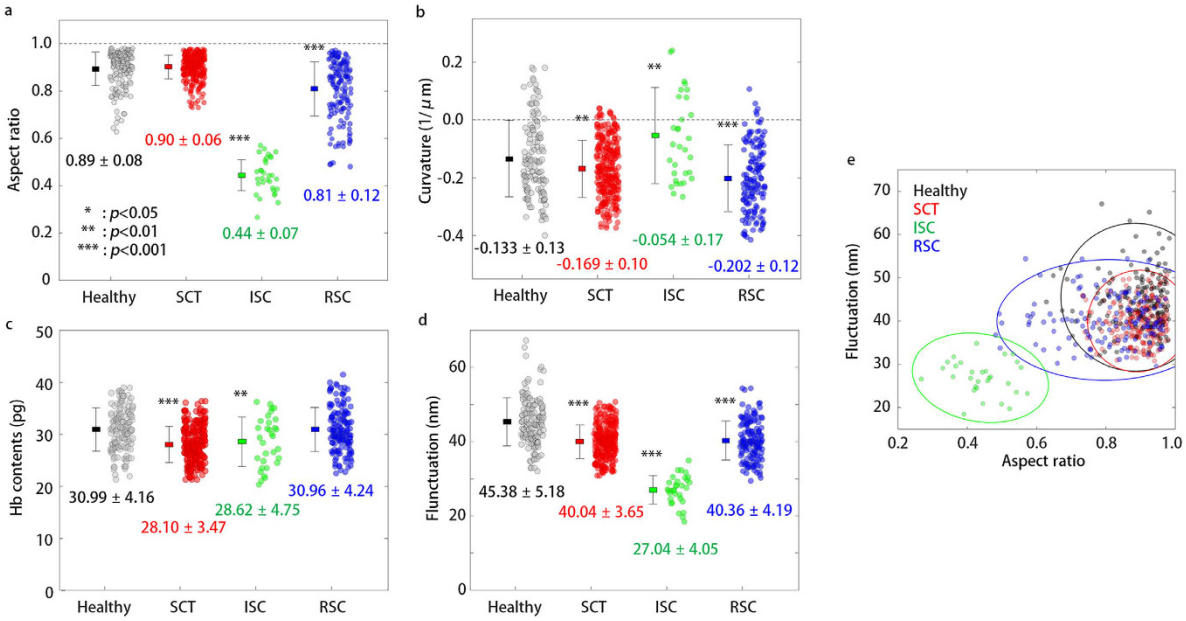

Figure 3. Measured morphological and mechanical parameters. (**a**) Aspect ratios of the projected areas of the cells. (**b**) Membrane curvatures of the center dimple regions. (**c**) Hb contents in individual cells. (**d**) Dynamic fluctuations in the cell membranes. (**e**) A scatter plot of the dynamic membrane fluctuation versus cell aspect ratio. Solid lines correspond to 95% confidence ellipses for each group. Statistical tests were performed with the Mann–Whitney *U*-tests (**a**) and Student's *t*-tests (**b**–**d**) against the Healthy group (*$p < 0.05$; **$p < 0.01$; ***$p < 0.001$). There are 135, 258, 30, 138 data points for Healthy, SCT, ISC, and RSC groups, respectively, in the figure.

Hemoglobin contents in the individual RBCs. The total mass of Hb inside RBCs is an important biochemical parameter indicating the capacity of oxygen transportation by the RBCs. Using the present method, the total amount of Hb inside individual RBCs, or the Hb contents, can be calculated from the quantitative phase images[44,45]. Because Hb represents the majority of the soluble proteins in RBCs, the Hb mass inside a cell can be related to the integration of the optical phase delay over the cell area as follows:

$$Hb \text{ contents} = C_{Hb} \int h(x, y) dA = \frac{\lambda}{2\pi\alpha} \int \Delta\phi(x, y) dA, \quad (1)$$

where α is the refractive index increment of Hb (0.002 dL/g)[46]; C_{Hb} is the Hb concentration in a RBC and $\int dA$ is the integration over the cell area A[47].

The mean values of the Hb contents were 30.99 ± 4.16, 28.10 ± 3.47, 28.62 ± 4.75 and 30.96 ± 4.24 pg for the healthy, SCT, ISC, and RSC groups, respectively (Fig. 3c). The mean Hb contents averaged over the RBCs correspond to the mean corpuscular hemoglobin (MCH), which is a medical parameter extensively used in the clinical laboratory. The mean value of the Hb contents of the healthy group was within the physiological level (27–33 pg). The Hb contents of the SCT and ISC groups were slightly decreased compared to the healthy RBCs, and the mean values of the Hb contents for every group were within the normal physiological range (27–33 pg). This result is in agreement with previous reports that there is no medically significant difference in Hb contents for SCT and SCD RBCs[48,49]. This is also verified in statistical analysis using the mean values of individual donor, as shown in the Supplementary Figure S3.

Cell membrane deformability of individual RBCs. To analyze the biomechanical properties of the RBCs, the dynamic membrane fluctuations of the RBCs in the four groups were quantified from the measured dynamic 2-D height fluctuation images. Dynamic fluctuation in RBC membranes, consisting of tens of nanometer displacements at millisecond temporal frequencies, reflects the biomechanical properties of RBCs, including the viscoelastic properties of the cell membrane cortex as well as the viscosity of the cytoplasm[50]. To represent the deformability of the RBCs, we calculated the temporal standard deviations of the dynamic membrane displacements and spatially averaged over a cell area as follows:

$$Fluctuation = \int \text{std}[\Delta h(x, y; t)] dA \quad (2)$$

where std indicates the temporal standard deviation.

The average values for the fluctuations were 45.38 ± 5.18, 40.04 ± 3.65, 27.04 ± 4.05 and 40.36 ± 4.19 nm for healthy, SCT, ISC, and RSC groups, respectively (Fig. 3d). The values of the membrane fluctuations for the healthy RBCs were the highest among the groups, and their values are comparable with previous reports[22–24]. The ISCs

exhibited significantly decreased membrane fluctuations indicating a reduced cell deformability; the results agree well with previous reports[18,19]. The membrane fluctuations of the RSCs were between the fluctuation of the healthy RBCs and ISCs in agreement with previous findings[13,18,51]. The SCT RBCs had a similar level of fluctuations as the RSCs, which is also consistent with recent reports[16,52,53]. Consistent results are also observed in the analysis using mean values of individual donors, as shown in Supplementary Figure S4.

Correlation between the shapes and deformability of the individual RBCs. The results above show that both elongated forms and reduced membrane deformability in RBCs are the distinct characteristics of the SCT and SCD. For further clarification, correlation analysis between the dynamic membrane fluctuation and the aspect ratio were performed at the individual cell level for the four groups (Fig. 3e). The ISCs population was clearly isolated from the other population, and the other groups shared overlaps in the scatter plot. Even though both SCT and RSC RBCs showed cell deformability comparable to the healthy RBCs, the SCT RBCs had aspect ratios comparable to the healthy RBCs whereas the RSC RBCs had slightly reduced aspect ratios. Additionally, in the scatter plot, the population of the SCT RBCs is a subset of the healthy RBCs, implying that the SCT RBCs are difficult to distinguish from healthy RBCs based on their morphological, biochemical, and mechanical properties.

Discussion

This study presents systematic cell analysis of RBCs in Tanzania using the QPIU. We performed optical measurements of multiple characteristics of RBCs collected from SCT and SCD individuals. To date, this is the first report to investigate using holographic microscopy or QPI techniques in a clinical setting in Africa. Despite the recent discoveries and developments of several biophotonic approaches targeted for translational medicine, the application to clinical studies in Africa has been difficult due to a lack of funds, facilities, and experts in African countries. This study performed in Tanzania clearly shows that QPI techniques can be transferred into local clinical environments in underdeveloped countries, which significantly expand the applicability and potentials of QPI techniques and provide new possibilities for research and diagnosis in environments with limited resources.

In this study, a systematic investigation of the morphological, biochemical, and mechanical properties of individual RBCs was performed. The collected RBCs were categorized into four groups, healthy, SCT, ISC, and RSC groups, depending on the genotypes of the donors and the cell morphology. For each RBC, the optical phase delay images were obtained, from which the morphological (cell aspect ratio and membrane curvature), biochemical (Hb contents), and biomechanical (dynamic membrane fluctuation) properties were retrieved and investigated.

The aspect ratios of the RBCs clearly showed the elongated shapes of the ISCs and the round shapes of the other RBCs. The RSCs had a broaden distribution for the aspect ratio which might be due to partially damaged membranes. The SCT RBCs showed almost identical round shapes with the healthy RBCs. In accordance with the similar shapes of the healthy and SCT RBCs and the RSCs, their membranes had the distinct curvatures of dimples. On the other hand, the membrane of the ISCs became flattened on average although some of the ISCs still exhibited strong dimpled membranes. The reduced curvatures of the ISCs were thought to be related to the damaged spectrin networks which are responsible for the dimple formation[54]. The detailed mechanism for the reduced curvature should be investigated with further experiments. For example, the QPI combined with optical tweezers could be used to study the relation between the membrane curvature and repeated elongation[55].

As a biochemical assessment, we measured the Hb contents inside the individual RBCs. The measured Hb contents of the SCT RBCs and ISCs were slightly lower ($<10\%$) than that of the healthy RBCs. However, the deviations did not seem to be medically significant because all MCHs for the four groups were still within the physiological range. This result is consistent with previous work which had reported the MCH of SCT and SCD RBCs were within the physiological ranges[48,49]. Thus, the minor difference in MCH was believed to originate from the biological variations of the individuals. An additional source for the different MCHs could be related to the different losses of Hb components during a RBC life span[56]. An important fact is that the similar values of MCH among the groups clearly indicate the comparable oxygen capacity of the individual RBCs regardless of the sickle genes. Thus, it is evident that anemia is developed by the lack of an RBC population and blocked capillaries rather than the reduced oxygen capacity of the individual cells.

The membrane fluctuation, the dynamic characteristics indicating the deformability of the cells, was quantified by investigating the dynamics of the cell height. The measured membrane fluctuations showed that the SCT and SCD RBCs had less deformability than that of the healthy RBCs. In particular, the ISCs had the smallest fluctuation which was due to the permanent change in the membrane cortex structures as a result of repeated sickling[52,57]. It is worth noticing that the SCT RBCs and RSCs had lower values for the fluctuations compared to the healthy RBCs despite the indistinguishable morphology from the healthy RBCs. The result suggests that the reduced deformability not be solely caused by the polymerization of HbS and raises the necessity for further study on the mechanism of membrane stiffening.

From the correlative analysis between the aspect ratio and the fluctuation, we reconfirmed that the reduced deformability and elongated shape are distinct properties of the ISCs. The ISCs had the lowest fluctuation and aspect ratio among the groups, suggesting a correlation between the elongation and fluctuation. One possible reason is that a low aspect ratio means a high bending energy stored in the lipid membrane, which could suppress dynamic membrane fluctuation.

In this experiment, we categorized the SCD RBCs into two types, ISCs and RSCs, according to the shape of the cells. However, the RBCs from SCD individuals are often classified into four or more groups depending on their Hb concentration. With the combination of appropriate density-based separation techniques and QPI techniques, we would be able to investigate the characteristics of the RBCs according to more specific conditions. Furthermore, non-contact optical measurements of the individual membrane fluctuation controlling the oxygen level of the sample solutions may provide new quantitative findings for the hemodynamic characteristics of the SCT and SCD RBCs.

The method presented in this study can be readily applied in other clinical settings in underdeveloped countries because the QPIU is cost-effective and easy-to-use. Building the prototype QPIU system used in this study cost less than $1,000 USD, but it can be further reduced significantly if cheaper optics are used and mass production is involved. Furthermore, no special training is required to operate the system because the QPIU is align-free and image analysis can be fully automated. Although the QPIU system has limited modality due to its simplicity, it can provide unique label-free and quantitative imaging capability for blood cells, parasites, and bacteria, which are important for the study and diagnosis of several neglected tropical diseases.

In summary, we have successfully demonstrated the practicality of the QPIU in Africa for the first time. We did measurements on the quantitative phase imaging of RBCs from individuals with SCD and SCT and investigated various cellular parameters. This study also showed that an existing simple bright-field microscope could be converted into a high-performance quantitative phase imaging instrument capable of measuring morphological, biochemical, and mechanical properties at the same time. This approach provides valuable information to clinics which has been usually obtained with complete blood counter and cell biomechanics experimental apparatuses such as micropipette aspiration, which is difficult to implement and do in local clinics in underdeveloped countries.

We believe it is a perfect time to transfer the QPIU technique to underdeveloped countries as the awareness about the clinical and economic burdens of SCD increases. This demonstration suggests that the QPIU is an important and potential tool because the technique is cost-effective, compact, easy-to-use, and does not require expensive reagents or consumables. These advantages obviously provide additional opportunities for studying other parasitic and bacterial epidemics and will finally significantly contribute to the improvement of these health conditions in Africa. We believe that our demonstration in Tanzania presents an important and promising example of transferring advanced technology from the laboratory to the practical field.

Materials and Methods

Recruitment procedures. The sample preparation procedures and the methods were approved by the Medical Research Coordinating Committee of the National Institute for Medical Research (reference number: NIMR/HQ/R.8a/Vol. IX/1896) and the Institutional Review Board (IRB project number: KH2015–37). The study was conducted as a part of an ongoing hospital-based acute febrile illness study and done at the National Institute for Medical Research (NIMR) laboratory, located within Morogoro Regional Referral Hospital, Tanzania. Participants were recruited from the patients admitted to the pediatric ward number 6, and the remaining ones were patients who presented to the outpatient department with fever and other symptoms to seek treatment. Relatives of admitted participants also assisted in inviting other known sickle cell patients who were also requested to take part in the study. The remaining participants were healthy individuals who volunteered to take part in. Verbal consent was obtained from all study participants and the parents or guardian of recruited children before any sample collections. All study participants were tested for malaria using malaria rapid diagnostic tests (05FK60, Standard Diagnostics, Inc.) to minimize the chances of creating confusion with the effect of malaria. It has been suggested that malaria infection particularly *P. falciparum* parasites alters the characteristics of the cell membrane[24].

Genotyping by sequencing polymerase chain reaction (PCR) products. The sickle genotypes (AA, AS and SS) of the patients were confirmed by DNA sequencing of the PCR products of the beta-globin gene region including the sickle single nucleotide polymorphism (SNP)[58]. The genomic DNA was purified from 500 μl of whole blood with a commercial kit. The sickle SNP, A/T transversion in the codon 6 of the human beta-globin gene, was determined by DNA sequencing with the Big Dye Terminator sequencing kit (ABI). A 520 bp PCR product of the gene region including the sickle SNP loci was amplified with primers (Sickle_F: AAAGTCAGGGCAGAGCCATC; Sickle_R: AAGGGTCCCATAGACTCACCC), with 30 cycles of 94 °C for 30 sec., 55 °C for 30 sec., 72 °C for 60 sec. The corresponding PCR fragment was purified from the agarose gel and subjected to DNA sequencing.

Sample preparations. Under aseptic procedures, approximately 1 mL of peripheral blood was collected from the *participants* (known sickle cell patients and their biological parents and blood relatives). Specimens were collected in vacutainers tubes containing EDTA anticoagulant. All samples were stored at room temperature for a maximum of 10 hours before the measurements were conducted. The whole blood samples were diluted 500 times in phosphate buffered saline (PBS, Welgene Inc.) solution. The diluted blood solutions (5 μL) were injected into glass channels made of slide glass and a KOH-washed coverslip. Double-sided tapes of 100 μm thicknesses (3M Company) were used for spacers in the channels. The blood samples were considered to be under an oxygenated condition because no chemicals for deoxygenation were used, and the blood samples were sufficiently exposed to oxygen in the air.

Calculating the RBC height from the optical phase images. The height of the RBC is obtained from $\Delta\phi(x, y, t)$ through the equation: $\Delta\phi(x, y, t) = 2\pi/\lambda \cdot \Delta n \cdot h(x, y, t)$, where λ is the wavelength of light in a vacuum ($\lambda = 532$ nm) and Δn is the refractive index contrast between an RBC and a medium (i.e., PBS solution). In this experiment, because the refractive index contrast can be considered to be solely originating from the Hb inside the RBCs, the refractive index contrast could be expressed as $\Delta n = \alpha \cdot C_{Hb}$[45,59], where C_{Hb} is the Hb concentration, and α is the refractive index increment of the Hb ($\alpha = 0.002$ dL/g[46]). Because we were not able to measure C_{Hb} for the individual RBCs at the clinic, the values of C_{Hb} were adapted from previous reports to determine Δn. Specifically, for the healthy and SCT RBCs which have a physiological concentration of Hb, we used $C_{Hb} = 34$ g/dL[46,48]. For the SCD RBCs, two different C_{Hb} values were used depending on the groups because the Hb concentration of the SCD RBCs is a bimodal distribution[33,60]. One population, mainly comprised of the RSCs, is known

to have an average Hb concentration similar to that of the healthy RBCs ($C_{Hb} = 34$ g/dL). The other population, mainly comprised of the ISCs, is known to have an average concentration of 45 g/dL[33]. Thus, the optical phase delay of 1 radian corresponds to the height of 1.249 μm for the healthy and SCT RBCs and RSCs and a height of 0.944 μm for the ISCs.

Calculating the membrane curvature. To quantify the membrane curvature of the individual cells, a mean curvature, which is the mean of two principal curvatures, at each point on the cells was calculated from the height map. The calculated mean curvatures at each point were averaged over a dimple region around the center of the cells. The dimple region is defined by an elliptical area whose diameters are 40% of the diameters of the individual RBCs.

References

1. Pauling, L., Itano, H. A., Singer, S. & Wells, I. C. Sickle cell anemia, a molecular disease. *Science* **110,** 543–548 (1949).
2. Stuart, M. J. & Nagel, R. L. Sickle-cell disease. *The Lancet* **364,** 1343–1360 (2004).
3. PediatriaAshley-Koch, A., Yang, Q. & Olney, R. S. Sickle hemoglobin (Hb S) allele and sickle cell disease: a HuGE review. *American Journal of Epidemiology* **151,** 839–845 (2000).
4. Roseff, S. Sickle cell disease: a review. *Immunohematology/American Red Cross* **25,** 67–74 (2008).
5. Kark, J. A., Posey, D. M., Schumacher, H. R. & Ruehle, C. J. Sickle-cell trait as a risk factor for sudden death in physical training. *New England Journal of Medicine* **317,** 781–787 (1987).
6. Harris, K. M., Haas, T. S., Eichner, E. R. & Maron, B. J. Sickle cell trait associated with sudden death in competitive athletes. *The American journal of cardiology* **110,** 1185–1188 (2012).
7. World Health Organization. *Sickle-cell anaemia: Report by the Secretariat*. (2006).
8. Makani, J. *et al.* Mortality in sickle cell anemia in Africa: a prospective cohort study in Tanzania. *PLoS One* **6,** e14699 (2011).
9. Neel, J. V. In *Racial and ethnic differences in the health of older Americans* (eds Soldo, Beth J. & Martin, Linda G) Ch. 7, 211 (National Academies Press, 1997).
10. Grosse, S. D. *et al.* Sickle Cell Disease in Africa: A Neglected Cause of Early Childhood Mortality. *American Journal of Preventive Medicine* **41,** S398–S405, doi: 10.1016/j.amepre.2011.09.013 (2011).
11. Centers for Disease Control and Prevention. Mortality among children with sickle cell disease identified by newborn screening during 1990–1994–California, Illinois, and New York. *Morbidity and mortality weekly report* **47,** 169 (1998).
12. Barabino, G. A., Platt, M. O. & Kaul, D. K. Sickle cell biomechanics. *Annual review of biomedical engineering* **12,** 345–367 (2010).
13. Nash, G., Johnson, C. & Meiselman, H. Mechanical properties of oxygenated red blood cells in sickle cell (HbSS) disease. *Blood* **63,** 73–82 (1984).
14. Messer, M. J. & Harris, J. W. Filtration characteristics of sickle cells: rates of alteration of filterability after deoxygenation and reoxygenation, and correlations with sickling and unsickling. *Journal of Laboratory and Clinical Medicine* **76,** 537–547 (1970).
15. Barabino, G., McIntire, L., Eskin, S., Sears, D. & Udden, M. Endothelial cell interactions with sickle cell, sickle trait, mechanically. *Blood* **70,** 152–157 (1987).
16. Brandão, M. M. *et al.* Optical tweezers for measuring red blood cell elasticity: application to the study of drug response in sickle cell disease. *European Journal of Haematology* **70,** 207–211, doi: 10.1034/j.1600-0609.2003.00027.x (2003).
17. Maciaszek, J. L. & Lykotrafitis, G. Sickle cell trait human erythrocytes are significantly stiffer than normal. *Journal of Biomechanics* **44,** 657–661, doi: 10.1016/j.jbiomech.2010.11.008 (2011).
18. Shaked, N. T., Satterwhite, L. L., Telen, M. J., Truskey, G. A. & Wax, A. Quantitative microscopy and nanoscopy of sickle red blood cells performed by wide field digital interferometry. *Journal of biomedical optics* **16,** 030506 (2011).
19. Byun, H. *et al.* Optical measurement of biomechanical properties of individual erythrocytes from a sickle cell patient. *Acta Biomater*. (2012).
20. Popescu, G. *Quantitative Phase Imaging of Cells and Tissues*. (McGraw-Hill Professional, 2011).
21. Lee, K. *et al.* Quantitative phase imaging techniques for the study of cell pathophysiology: from principles to applications. *Sensors* **13,** 4170–4191 (2013).
22. Park, Y. *et al.* Metabolic remodeling of the human red blood cell membrane. *Proceedings of the National Academy of Sciences* **107,** 1289 (2010).
23. Park, Y. *et al.* Measurement of red blood cell mechanics during morphological changes. *Proceedings of the National Academy of Sciences* **107,** 6731 (2010).
24. Park, Y. K. *et al.* Refractive index maps and membrane dynamics of human red blood cells parasitized by Plasmodium falciparum. *P Natl Acad Sci USA* **105,** 13730–13735, doi: 10.1073/pnas.0806100105 (2008).
25. Park, H. *et al.* Three-dimensional refractive index tomograms and deformability of individual human red blood cells from cord blood of newborn infants and maternal blood. *J. Biomed. Opt.* **20,** 111208, doi: 10.1117/1.jbo.20.11.111208 (2015).
26. Park, H. *et al.* Characterizations of individual mouse red blood cells parasitized by Babesia microti using 3-D holographic microscopy. *Scientific Reports* **5,** doi: 10.1038/srep10827.
27. Charriere, F. *et al.* Living specimen tomography by digital holographic microscopy: morphometry of testate amoeba. *Optics Express* **14,** 7005–7013, doi: 10.1364/Oe.14.007005 (2006).
28. Rappaz, B. *et al.* Spatial analysis of erythrocyte membrane fluctuations by digital holographic microscopy. *Blood Cells, Molecules, and Diseases* **42,** 228–232 (2009).
29. Lee, K. & Park, Y. Quantitative phase imaging unit. *Optics Letters* **39,** 3630–3633 (2014).
30. Debnath, S. K. & Park, Y. Real-time quantitative phase imaging with a spatial phase-shifting algorithm. *Optics letters* **36,** 4677–4679 (2011).
31. Kim, Y. *et al.* Common-path diffraction optical tomography for investigation of three-dimensional structures and dynamics of biological cells. *Optics express* **22,** 10398–10407 (2014).
32. Lux, S. E., JoHN, K. M. & Karnovsky, M. Irreversible deformation of the spectrin-actin lattice in irreversibly sickled cells. *Journal of Clinical Investigation* **58,** 955 (1976).
33. Kaul, D. K., Fabry, M., Windisch, P., Baez, S. & Nagel, R. Erythrocytes in sickle cell anemia are heterogeneous in their rheological and hemodynamic characteristics. *Journal of clinical investigation* **72,** 22–31 (1983).
34. Kumar, A. A. *et al.* Density-based separation in multiphase systems provides a simple method to identify sickle cell disease. *Proceedings of the National Academy of Sciences* **111,** 14864–14869, doi: 10.1073/pnas.1414739111 (2014).
35. Popescu, G. *et al.* Erythrocyte structure and dynamics quantified by Hilbert phase microscopy. *J. Biomed. Opt.* **10,** 060503 (2005).
36. Popescu, G. *et al.* Imaging red blood cell dynamics by quantitative phase microscopy. *Blood Cells Mol Dis* **41,** 10–16, doi: 10.1016/j.bcmd.2008.01.010 (2008).
37. Kim, Y., Kim, K. & Park, Y. In *Blood Cell - An Overview of Studies in Hematology* (ed Moschandreou, Terry E.) Ch. 10, 167–194 (INTECH, 2012).
38. Park, Y., Best, C. A. & Popescu, G. In *Mechanobiology of Cell-cell and Cell-matrix Interactions* 279–309 (Springer, 2011).

39. Park, Y. *et al.* Measurement of the nonlinear elasticity of red blood cell membranes. *Phys. Rev. E* **83,** doi: 10.1103/PhysRevE.83.051925 (2011).
40. Chandramohanadas, R. *et al.* Biophysics of malarial parasite exit from infected erythrocytes. *PLoS One* **6,** e20869, doi: 10.1371/journal.pone.0020869 (2011).
41. Diez-Silva, M. *et al.* Pf155/RESA protein influences the dynamic microcirculatory behavior of ring-stage Plasmodium falciparum infected red blood cells. *Scientific reports* **2** (2012).
42. Park, H. *et al.* 3-D refractive index tomograms and deformability of individual human red blood cells from cord blood of newborn infants and maternal blood. *arXiv preprint arXiv:1505.04232* (2015).
43. de Jong, K., Larkin, S. K., Styles, L. A., Bookchin, R. M. & Kuypers, F. A. Characterization of the phosphatidylserine-exposing subpopulation of sickle cells. *Blood* **98,** 860–867 (2001).
44. Barer, R. & Tkaczyk, S. *Refractive index of concentrated protein solutions*. (1954).
45. Park, Y., Yamauchi, T., Choi, W., Dasari, R. & Feld, M. S. Spectroscopic phase microscopy for quantifying hemoglobin concentrations in intact red blood cells. *Optics letters* **34,** 3668–3670 (2009).
46. Faber, D. J. *et al.* Oxygen saturation-dependent absorption and scattering of blood. *Physical review letters* **93,** 028102 (2004).
47. Popescu, G. *et al.* Optical imaging of cell mass and growth dynamics. *Am J Physiol Cell Physiol* **295,** C538–544, doi: 10.1152/ajpcell.00121.2008 (2008).
48. Ashcroft, M. T., Miall, W. E. & Milner, P. A comparison between the characteristics of Jamaican adults with normal hemoglobin and those with sickle cell trait. *American Journal of Epidemiology* **90,** 236–243 (1969).
49. Akinbami, A. *et al.* Haematological values in homozygous sickle cell disease in steady state and haemoglobin phenotypes AA controls in Lagos, Nigeria. *BMC research notes* **5,** 396 (2012).
50. Popescu, G. *et al.* Imaging red blood cell dynamics by quantitative phase microscopy. *Blood Cells Mol. Dis.* **41,** 10–16 (2008).
51. Evans, E. A. & Mohandas, N. Membrane-associated sickle hemoglobin: a major determinant of sickle erythrocyte rigidity. *Blood* **70,** 1443–1449 (1987).
52. Maciaszek, J. L., Andemariam, B. & Lykotrafitis, G. Microelasticity of red blood cells in sickle cell disease. *The Journal of Strain Analysis for Engineering Design* **46,** 368–379 (2011).
53. Zheng, Y. *et al.* Mechanical differences of sickle cell trait (SCT) and normal red blood cells. *Lab on a Chip* **15,** 3138–3146, doi: 10.1039/C5LC00543D (2015).
54. Mohandas, N. & Gallagher, P. G. Red cell membrane: past, present, and future. *Blood* **112,** 3939–3948 (2008).
55. Dao, M., Lim, C. & Suresh, S. Mechanics of the human red blood cell deformed by optical tweezers. *Journal of the Mechanics and Physics of Solids* **51,** 2259–2280 (2003).
56. Willekens, F. L. A. *et al.* Hemoglobin loss from erythrocytes *in vivo* results from spleen-facilitated vesiculation. *Blood* **101,** 747–751, doi: 10.1182/blood-2002-02-0500 (2003).
57. Hebbel, R. Beyond hemoglobin polymerization: the red blood cell membrane and sickle disease pathophysiology. *Blood* **77,** 214–237 (1991).
58. Saiki, R. K. *et al.* Enzymatic amplification of beta-globin genomic sequences and restriction site analysis for diagnosis of sickle cell anemia. *Science* **230,** 1350–1354 (1985).
59. Barer, R. & Joseph, S. Refractometry of living cells. *Journal of Cell Science* **95,** 399–423 (1954).
60. Fabry, M. & Nagel, R. Heterogeneity of red cells in the sickler: a characteristic with practical clinical and pathophysiological implications. *Blood cells* **8,** 9–15 (1981).

Acknowledgements

This work was supported by KAIST, and the National Research Foundation of Korea (2015R1A3A2066550, 2014K1A3A1A09063027, 2012-M3C1A1-048860, 2014M3C1A3052537) and Innopolis foundation (A2015DD126). We thank all study participants who accepted to take part in this study.

Author Contributions

Y.P. and D.-J.K. conceived the idea and directed the work. L.E.M. performed experiments and wrote the main manuscript. J.J., K.L., K.K. and J.Y. designed optics system and discuss results. P.E.K. and J.J.M. prepared RBC samples. All authors reviewed the manuscript.

Additional Information

Supplementary information accompanies this paper at http://www.nature.com/srep

Competing financial interests: The authors declare no competing financial interests.

How to cite this article: Jung, J. *et al.* Optical characterization of red blood cells from individuals with sickle cell trait and disease in Tanzania using quantitative phase imaging. *Sci. Rep.* **6**, 31698; doi: 10.1038/srep31698 (2016).